



# High-performance cavity-enhanced quantum memory with warm atomic cell

Lixia Ma<sup>1,3</sup>, Xing Lei<sup>1,3</sup>, Jieli Yan<sup>1</sup>, Ruiyang Li<sup>1</sup>, Ting Chai<sup>1</sup>, Zhihui Yan<sup>1,2</sup> <sup>✉</sup>, Xiaojun Jia<sup>1,2</sup> <sup>✉</sup>, Changde Xie<sup>1,2</sup> & Kunchi Peng<sup>1,2</sup>

High-performance quantum memory for quantized states of light is a prerequisite building block of quantum information technology. Despite great progresses of optical quantum memories based on interactions of light and atoms, physical features of these memories still cannot satisfy requirements for applications in practical quantum information systems, since all of them suffer from trade-off between memory efficiency and excess noise. Here, we report a high-performance cavity-enhanced electromagnetically-induced-transparency memory with warm atomic cell in which a scheme of optimizing the spatial and temporal modes based on the time-reversal approach is applied. The memory efficiency up to  $67 \pm 1\%$  is directly measured and a noise level close to quantum noise limit is simultaneously reached. It has been experimentally demonstrated that the average fidelities for a set of input coherent states with different phases and amplitudes within a Gaussian distribution have exceeded the classical benchmark fidelities. Thus the realized quantum memory platform has been capable of preserving quantized optical states, and is ready to be applied in quantum information systems, such as distributed quantum logic gates and quantum-enhanced atomic magnetometry.

<sup>1</sup>State Key Laboratory of Quantum Optics and Quantum Optics Devices, Institute of Opto-Electronics, Shanxi University, Taiyuan 030006, P. R. China.

<sup>2</sup>Collaborative Innovation Center of Extreme Optics, Shanxi University, Taiyuan 030006, P. R. China. <sup>3</sup>These authors contributed equally: Lixia Ma, Xing Lei.

✉email: [zhyan@sxu.edu.cn](mailto:zhyan@sxu.edu.cn); [jjaxj@sxu.edu.cn](mailto:jjaxj@sxu.edu.cn)

The high-performance quantum memory featuring both high memory efficiency and low excess noise is an indispensable building block in quantum information systems, distributed quantum computation and quantum metrology. For example, the multiple spatial separated macroscopic objects can be entangled by efficiently storing multipartite entangled state of optical modes, and its realization depends on memory efficiency and noise level<sup>1</sup>. In distributed quantum computation, enhancing the memory fidelity among entangled different modules (nodes) is significant for implementing optical logical gates<sup>2,3</sup>. It has been demonstrated that the atom-based measurement sensitivity is ultimately restricted by the quantum noise limit (QNL), and spin squeezing holds a promise to overcome this restriction<sup>4,5</sup>. In quantum-enhanced atomic magnetometry, the spin squeezing can be generated by efficiently storing the squeezed optical mode, and then used to measure weak signal merged in the quantum noise<sup>6</sup>.

Over the past decades, various light-atom interactions have been utilized to implement quantum memory, such as electromagnetically induced transparency (EIT)<sup>7–12</sup>, far-off-resonance Raman<sup>13</sup>, quantum non-demolition<sup>14</sup>, Autler–Townes splitting<sup>15</sup> and photon echo interaction<sup>16</sup>. By applying a gradient magnetic field in an atomic cell operating with a special regime, gradient echo memory provides the storage of coherent pulses containing around one photon with the recall fidelity up to 98%<sup>17</sup>. The high memory efficiency is crucially important for practical quantum information<sup>18,19</sup>. Toward the aim of high efficiency, the coherent optical storage efficiency has reached  $92.0 \pm 1.5\%$  in an optically dense cold atomic media based on EIT effect; however, the excess noise attached to the signal mode is about 6% higher than the QNL<sup>20</sup>. The memory efficiency in warm atomic cell has also been improved by using optimal input signal mode<sup>21</sup>. Besides, another challenge for the memory of quantized optical states is to suppress the excess noise, which will destroy quantum features of stored states. In the processing of atom-light interaction with a  $\Lambda$ -type energy configuration, the coupling of the control mode on the signal mode transition will induce unwanted four-wave-mixing (FWM) noise, which is the main noise source of quantum memory<sup>22,23</sup>. In near-resonant EIT memory with a moderate atomic number, the interaction for storing quantum states is dominant and the influence of FWM noise is relatively less. The EIT memory in the warm atomic vapor with the noise of 2% higher than the QNL and the completed storage amplitude efficiency of 10% has been reported<sup>24</sup>. It has been proved that EIT memories are able to reach the QNL, which have been applied to preserve the squeezed light with atomic ensemble<sup>25,26</sup>. Alternatively, the optical cavity can enhance the light-atom interaction<sup>27–33</sup> and suppress the excess noise<sup>34</sup>. Although in a demonstrated cavity-enhanced Raman memory the FWM noise has been effectively suppressed, the memory efficiency is below 10%<sup>22</sup>. So far, the effective realization of quantum memory with both high efficiency and low noise approaching the QNL is still a significant challenge for practical applications.

To accomplish quantum memory with the necessary features of both high memory efficiency and low excess noise, we present an experimental demonstration on a cavity-enhanced EIT memory in a simple warm atomic cell, in which the near-perfect mode matching technique based on time-reversal approach is applied<sup>21</sup>. In this way, not only the FWM noise but also the other noises are actively suppressed, due to off resonance with optical cavity; while the memory interaction is effectively enhanced, by resonating the signal mode in the optical cavity. Thanks to the cavity-enhanced EIT interaction and the near-perfect mode matching, both high memory efficiency up to  $67 \pm 1\%$  and low noise level close to the QNL are simultaneously obtained by the memory system. Based on both high efficiency and low excess noise at QNL level, the

average fidelities of the memory measured on a set of input coherent states with varied phases and amplitudes within a Gaussian distribution have totally exceeded the corresponding classical benchmark fidelities. Thus, the performance of the memory has reached a level higher than any classical memory and is able to store quantum states of light<sup>35,36</sup>.

## Results

**Principle of cavity-enhanced quantum memory.** In quantum optics, the optical mode is represented by the annihilation operator  $\hat{a}$ , the amplitude (phase) quadrature  $\hat{X}_L(\hat{Y}_L)$  of light corresponds to the real (imaginary) part of the annihilation operator  $\hat{a}$ , as  $\hat{X}_L = (\hat{a} + \hat{a}^\dagger)/\sqrt{2}$  ( $\hat{Y}_L = (\hat{a} - \hat{a}^\dagger)/\sqrt{2}i$ )<sup>37</sup>. Under the Holstein–Primakoff approximation, the collective atomic spin wave is described by the lowering operator  $\hat{S} = \sum_i |g\rangle\langle m|$ , here  $|g\rangle$  and  $|m\rangle$  stand for a ground state and meta-stable state, respectively. The amplitude (phase) quadrature  $\hat{X}_A(\hat{Y}_A)$  of the atoms is associated with the  $y(z)$  component of the Stokes operator  $\hat{S}_y(\hat{S}_z)$  on the Bloch sphere, which is represented by  $\hat{X}_A = (\hat{S} + \hat{S}^\dagger)/\sqrt{2} = \hat{S}_y/\sqrt{\langle \hat{S}_x \rangle}$  ( $\hat{Y}_A = (\hat{S} - \hat{S}^\dagger)/\sqrt{2}i = \hat{S}_z/\sqrt{\langle \hat{S}_x \rangle}$ )<sup>14</sup>. The coherent state of light is a minimum uncertainty state with equal uncertainty between two conjugate quadrature components, which is usually used to describe the quantized state of laser. The quantum nature of an optical memory can be characterized by means of preserving coherent state, thus the coherent state of optical mode is utilized as the input state of quantum memory in our experiment. The quantized state can be transferred between light and atomic superposition in the EIT memory<sup>8</sup>. The  $\Lambda$ -type three-level system of a ground state  $|g\rangle$ , a meta-stable state  $|m\rangle$  and an excited state  $|e\rangle$  is employed in the EIT configuration, which is presented in the insert of Fig. 1a. The signal mode is near resonant with the transition between a ground state  $|g\rangle$  and an excited state  $|e\rangle$ , while control mode is near resonant with the transition between a meta-stable state  $|m\rangle$  and an excited state  $|e\rangle$ . In our system, the control mode is much stronger than the signal mode, and is treated as a classical mode. When the collective atomic spin wave  $\hat{S}(t)$  interacts with the signal mode  $\hat{a}(t)$  via EIT process, the quantized state of the signal mode and the atomic ensemble can be transferred to each other, because the effective Hamiltonian  $\hat{H}_{EIT}$  of light-atom interaction is a type of beam-splitter interaction<sup>38</sup>. The quantum memory process includes three stages of writing, storage, and reading that are implemented by modulating the light-atom interaction with a control mode. Therefore, the step-like function used as an approximation of switching on and off processes in EIT interaction can be shown as follows:  $\hat{H}(t) = \hbar\kappa\hat{a}^\dagger\hat{S} + \hbar\kappa\hat{S}^\dagger\hat{a}$  ( $-\infty < t < 0$ );  $\hat{H}(t) = 0$  ( $0 < t < T_0$ );  $\hat{H}(t) = \hbar\kappa\hat{a}^\dagger\hat{S} + \hbar\kappa\hat{S}^\dagger\hat{a}$  ( $T_0 < t < \infty$ ), where  $T_0$  is the storage time,  $\kappa = \sqrt{N_a}\mu\Omega/\Delta$  is the effective light-atom interaction constant,  $N_a$  is the atomic number,  $\mu$  is the light-atom coupling constant,  $\Omega$  is the Rabi frequency of the control mode, and  $\Delta$  is the detuning between light and atom coupling.

Figure 1a is a diagram for the cavity-enhanced quantum memory with a warm atomic cell. The cavity with a bow-tie-type ring configuration consists of two plano mirrors and two concave mirrors, which enables to enhance the light-atom interaction and suppress the excess noise. The input signal mode  $\hat{A}(t)^{in}$  is coupled into the cavity mode  $\hat{a}$  through the input–output mirror with the coupling rate to the cavity of input mode  $\gamma_1 = T/(2\tau)$ , where  $T$  is the transmission of input–output mirror and  $\tau$  is the round-trip time of the optical mode inside optical cavity. The other three cavity mirrors are highly reflective for the optical signal mode, and one of them is mounted on piezoelectric transducer for

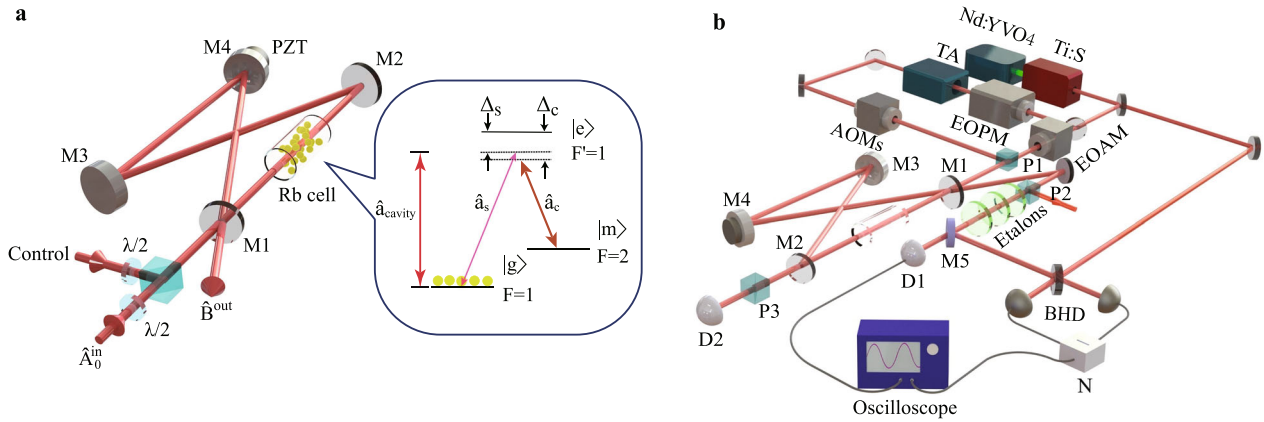


**Fig. 1 Schematic diagram.** **a** Diagram for the cavity-enhanced quantum memory and atomic energy level for quantum memory. Atoms with a ground state  $|g\rangle: |5S_{1/2}, F = 1\rangle$ , a meta-stable state  $|m\rangle: |5S_{1/2}, F = 2\rangle$ , and an excited state  $|e\rangle: |5P_{1/2}, F = 1\rangle$  are shown. The atomic cell is placed between two plano mirrors, where the optical cavity simultaneously enhances the light-atom interaction and suppresses the excess noise. **b** Experimental setup for implementing cavity-enhanced quantum memory. TA tapered amplifier, PZT piezoelectric transducer, EOAM electro-optical amplitude modulator, EOPM electro-optical phase modulator, AOM acousto-optical modulator, BHD balanced homodyne detector, D photoreceiver detector, M mirror, P Glan-Thompson polarizer, N negative power combiner.

scanning or locking the cavity length. The cavity loss  $L$  is unavoidable in real experiment due to the imperfect coating, and the corresponding decay rate of cavity loss is  $\gamma_2 = L/(2\tau)$ , which introduces the vacuum noise  $\hat{A}(t)_v^{in}$ . The atomic spin wave decoherence rate is  $\gamma_0$ , and couples the noise of atomic medium  $\hat{S}(t)_v$  into cavity mode  $\hat{a}$ . When the input signal mode resonates with cavity mode and the control mode is near-resonance with the cavity mode, the FWM noise is off-resonance and effectively suppressed. Quantum Langevin equations, describing evolution of observable operators for the cavity mode  $\hat{a}(t)$  and collective atomic spin wave  $\hat{S}(t)$  are shown as

$$\frac{d\hat{a}(t)}{dt} = -\gamma\hat{a}(t) - i\kappa(t)\hat{S}(t) + \sqrt{2\gamma_1}\hat{A}(t)^{in} + \sqrt{2\gamma_2}\hat{A}(t)_v^{in}, \quad (1)$$

$$\frac{d\hat{S}(t)}{dt} = -\gamma_0\hat{S}(t) - i\kappa(t)\hat{a}(t) + \sqrt{2\gamma_0}\hat{S}(t)_v, \quad (2)$$

where  $\gamma = \gamma_1 + \gamma_2$  corresponds to the sum of the coupling rate and the decay rate of cavity. For an input signal mode to be stored, a complete mode expansion into the longitudinal modes of the input optical mode is expressed by  $\hat{A}(t)^{in} = u(t)_0^{in}\hat{a}_0^{in}$ , where  $\hat{a}_0^{in}$  is an optical mode operator and  $u(t)_0^{in}$  is a temporal mode function of the input optical mode, which determines the optical mode shape. The input mode is dynamically shaped in time to provide optimum memory efficiency, and the temporal mode function in our system is approximately described by a rising exponential function<sup>39</sup>. In the cavity-enhanced memory system, the memory efficiency is defined as the ratio of the photon number of the released signal mode to that of the input signal mode, which depends on storage mechanism, media property and systematic losses. By solving quantum Langevin equations with the proper input temporal mode function, the memory efficiency  $\eta(T_0)$  at the storage time  $T_0$  from input optical mode to released optical mode is given by<sup>40</sup>

$$\eta(T_0) = \frac{(-\gamma_1\gamma_0^2e^{-\gamma T_0} + \gamma_1\kappa^2e^{-\gamma_0 T_0})^2}{(\gamma_0 + \gamma)^2(\kappa^2 + \gamma_0\gamma)^2}. \quad (3)$$

**Experimental realization of cavity-enhanced quantum memory.** Figure 2a shows the experimentally measured photon fluxes of the input and released signal modes at the storage time of 100 ns, when the atomic cell is heated to around 95 °C. The red

line and the blue line indicate the photon fluxes of the input signal mode and the released signal mode from the cavity-enhanced quantum memory system, respectively. The photon fluxes of the signal mode released from the memory system after passing through a filter system consisting of the polarizer and etalons with the external transmission of 85.6% is measured, thus the memory efficiency of  $67 \pm 1\%$  is directly measured and real memory efficiency deducting the external transmission losses should be  $78 \pm 1\%$ .

In the quantum memory, the fidelity  $F = \{Tr[(\hat{\rho}_1^{1/2}\hat{\rho}_2\hat{\rho}_1^{1/2})^{1/2}]\}^2$ , which describes the overlap of input states  $\hat{\rho}_1$  and the states  $\hat{\rho}_2$  released from the memory system, quantifies the performance of a quantum memory. Generally, if the average fidelities for a set of input coherent states within a Gaussian distribution surpass the classical benchmark fidelities, the quantum property outperforming classical systems can be verified<sup>41,42</sup>. Figure 2b presents the dependence of average fidelity on mean photon number  $\bar{n}$  of the Gaussian distribution of input set of coherent states. Blue solid line represents the theoretical average fidelity, and the red dots are the corresponding experimentally measured results. The black dashed line is the corresponding classical benchmark fidelity. It shows that the average fidelity depends on the mean photon number of the Gaussian distribution of the input coherent state, and reaches  $0.97 \pm 0.01$  for the input coherent state with the same mean photon number 0.60 of the Gaussian distribution of the input set of states, where the corresponding benchmark fidelity is 0.73. We can see that for a set of coherent states within the mean photon number range from  $\bar{n} = 0$  to  $\bar{n} = 8.0$ , the average fidelities for each input state exceed its classical benchmark fidelity, thus the quantum property of the memory outperforming any classical memory is confirmed<sup>35,36</sup> (see Supplementary Note 5 for details).

The memory efficiency and the average fidelity as functions of storage time are shown in Fig. 2c, where the average fidelity is determined by storing and releasing of various input coherent states with  $\bar{n} = 0.60$ . Blue solid line and blue squares are the theoretical memory efficiency and the experimentally measured values, respectively; and red dotted line and red dots represent the theoretical average fidelity and experimentally measured results, respectively; the black dashed line stands for the classical benchmark fidelity. From blue solid line, the lifetime in the memory system with warm atomic cell of 1.2  $\mu$ s is obtained, which is mainly limited by the magnetic noise. We can see that all

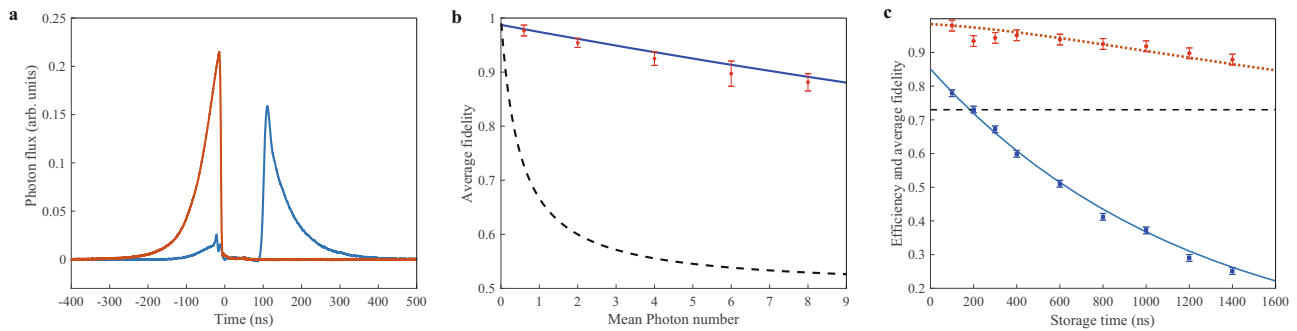


**Fig. 2 Experimental results.** **a** Temporal variation of the experimentally measured photon fluxes. The red line and the blue line indicate the photon fluxes of the input signal mode and the released signal mode from the cavity-enhanced quantum memory system, respectively. **b** The dependence of average fidelity on the mean photon number of the Gaussian distribution set of input coherent states. Blue solid line represents the theoretical average fidelity, and the red dots are the corresponding experimentally measured results. The black dashed line is the corresponding classical benchmark fidelity. **c** The results for memory efficiency and average fidelity vs. storage time. Blue solid line and blue squares are the theoretical memory efficiency and the experimentally measured values, respectively; and red dotted line and red dots represent the theoretical average fidelity and experimentally measured results, respectively; the black dashed line stands for the classical benchmark fidelity. Error bars represent  $\pm 1$  standard error are obtained with the statistics of the measured photon numbers and noises.

average fidelities are higher than the classical benchmark fidelities within the lifetime of atoms, and the storage time can be chosen arbitrarily within the lifetime.

## Discussion

Due to the use of an optical cavity with the near-perfect temporal and spatial matching, the memory efficiency of  $67 \pm 1\%$  and the excess noise close to QNL have been directly measured. For set of input coherent states within the mean photon number range from  $\bar{n} = 0$  to  $\bar{n} = 8.0$ , the deterministic average fidelities have exceeded the benchmark fidelities. Thus, the memory has entered into the quantum region. Because the atomic cell is put in the single layer magnetic field shielding barrel in the present experiment, the memory lifetime is short at the scale of microseconds due to the influence of the residual magnetic field noise. If the magnetic field noise is further reduced by employing the multiple-layer structure, the lifetime must be obviously increased<sup>43</sup>. Alternatively, it has been demonstrated that the cell-wall anti-relaxation coating onto the inner surface of the cell may provide an effective approach to extend the memory lifetime of warm atom to the scale of milliseconds<sup>5,44</sup>. We believe that if above mentioned feasible techniques are applied in our system, a quantum memory with longer memory lifetime will be possibly demonstrated based on the cavity-enhanced warm atomic system. The presented approach is achievable on a variety of other physical platforms, such as in trapped ions<sup>45–48</sup>, superconductors<sup>49–51</sup>, solid states<sup>52–55</sup> and optomechanics<sup>56–60</sup>.

For optical continuous-variable (CV) quantum information systems, the quantum information is encoded in the quadrature amplitudes and phases of optical signal modes, which have been used to implement quantum information protocols, such as quantum teleportation<sup>61</sup>, quantum dense coding<sup>62</sup> and quantum dense metrology<sup>63</sup>. For the presented memory experiment of optical coherent state, the quantum information is encoded and stored in the quadrature amplitudes and phases of optical signal modes. Besides, photons carrying information in discrete variable (DV), such as its arbitrary polarization state, can also be stored in the presented system by replacing the Glan–Thompson polarizer with a polarization insensitive beam splitter<sup>64</sup>. Thus, the cavity-enhanced memory works equally well for both CV and DV quantum information because the cavity-enhanced quantum memory is a linear mapping technique<sup>65</sup>. Quantized states of light, such as squeezing<sup>66</sup> and entanglement<sup>67</sup> are kernel

resources in quantum information science and technology, and the cavity-enhanced quantum memory system performs well enough to preserve quantum information of arbitrary quantized optical states. Due to the experimental simplicity of a warm atomic cell setup<sup>68,69</sup>, the presented system is robust and easily controlled, which is ready to be applied in some quantum information systems.

## Methods

**Experimental setup.** The experimental setup for implementing the cavity-enhanced quantum memory is shown in Fig. 1b, and the experimental details are given (see Supplementary Note 1). A <sup>87</sup>Rb atomic cell coated with 795 nm anti-reflection, which is placed in a magnetic shielding, is used as EIT medium of cavity-enhanced quantum memory system. An input signal mode with an optimized wave packet originally coming from Ti:sapphire laser is stored in an atomic cell inside the optical cavity. The time sequence of the cavity-enhanced quantum memory is given (see Supplementary Note 2). In this experiment, the photoreceiver detector D1 is applied to measure memory efficiency, which is theoretically analyzed in details (see Supplementary Note 3), and the excess noises can be analyzed from the BHD measurement (see Supplementary Note 4).

## Data availability

The data that support the findings of this study are available within the paper and its Supplementary information. Additional data are available from the corresponding authors upon reasonable request.

Received: 27 May 2021; Accepted: 14 April 2022;

Published online: 02 May 2022

## References

1. Yan, Z. et al. Establishing and storing of deterministic quantum entanglement among three distant atomic ensembles. *Nat. Commun.* **8**, 718 (2017).
2. Daiss, S. et al. A quantum-logic gate between distant quantum-network modules. *Science* **371**, 614–617 (2021).
3. Awschalom, D. et al. Development of Quantum Interconnects (QuICs) for next-generation information technologies. *PRX Quantum* **2**, 017002 (2021).
4. Lvovsky, A. I., Sanders, B. C. & Tittel, W. Optical quantum memory. *Nat. Photon.* **3**, 706–714 (2009).
5. Bao, H. et al. Spin squeezing of  $10^{11}$  atoms by prediction and retrodiction measurements. *Nature* **581**, 159–163 (2020).
6. Hald, J., Sorensen, J. L., Schori, C. & Polzik, E. S. Spin squeezed atoms: a macroscopic entangled ensemble created by light. *Phys. Rev. Lett.* **83**, 1319 (1999).
7. Fleischhauer, M. & Lukin, M. D. Dark-state polaritons in electromagnetically induced transparency. *Phys. Rev. Lett.* **84**, 5094 (2000).

8. Wang, Y. et al. Efficient quantum memory for single-photon polarization qubits. *Nat. Photon.* **13**, 346–351 (2019).
9. Vernaz-Gris, P., Huang, K., Cao, M., Sheremet, A. S. & Laurat, J. Highly-efficient quantum memory for polarization qubits in a spatially-multiplexed cold atomic ensemble. *Nat. Commun.* **9**, 363 (2018).
10. Kimble, H. J. The quantum internet. *Nature* **453**, 1023–1030 (2008).
11. Chanelière, T. et al. Storage and retrieval of single photons transmitted between remote quantum memories. *Nature* **438**, 833–836 (2005).
12. Eisaman, M. D. et al. Electromagnetically induced transparency with tunable single-photon pulses. *Nature* **438**, 837–841 (2005).
13. Ding, D. et al. Raman quantum memory of photonic polarized entanglement. *Nat. Photon.* **9**, 332–338 (2015).
14. Hammerer, K., Sorensen, A. S. & Polzik, E. S. Quantum interface between light and atomic ensembles. *Rev. Mod. Phys.* **82**, 1041 (2010).
15. Zhang, S. et al. Thermal-motion-induced non-reciprocal quantum optical system. *Nat. Photon.* **12**, 774–748 (2018).
16. Cho, Y. W. et al. Highly efficient optical quantum memory with long coherence time in cold atoms. *Optica* **3**, 100–107 (2016).
17. Hosseini, M., Campbell, G., Sparkes, B. M., Lam, P. K. & Buchler, B. C. Unconditional room-temperature quantum memory. *Nat. Phys.* **7**, 794–798 (2011).
18. Varnava, M., Browne, D. E. & Rudolph, T. Loss tolerance in one-way quantum computation via counterfactual error correction. *Phys. Rev. Lett.* **97**, 120501 (2006).
19. Grosshans, F. & Grangier, P. Quantum cloning and teleportation criteria for continuous quantum variables. *Phys. Rev. A* **64**, 010301 (2001).
20. Hsiao, Y. F. et al. Highly efficient coherent optical memory based on electromagnetically induced transparency. *Phys. Rev. Lett.* **120**, 183602 (2018).
21. Novikova, I. et al. Optimal control of light pulse storage and retrieval. *Phys. Rev. Lett.* **98**, 243602 (2007).
22. Saunders, D. J. et al. Cavity-enhanced room-temperature broadband Raman memory. *Phys. Rev. Lett.* **116**, 090501 (2016).
23. Wolters, J. et al. Simple atomic quantum memory suitable for semiconductor quantum dot single photons. *Phys. Rev. Lett.* **119**, 060502 (2017).
24. Cviklinski, J. et al. Reversible quantum interface for tunable single-sideband modulation. *Phys. Rev. Lett.* **101**, 133601 (2008).
25. Honda, K. et al. Storage and retrieval of a squeezed vacuum. *Phys. Rev. Lett.* **100**, 093601 (2008).
26. Appel, J., Figueroa, E., Korystov, D., Lobino, M. & Lvovsky, A. I. Quantum memory for squeezed light. *Phys. Rev. Lett.* **100**, 093602 (2008).
27. Vasilakis, G. et al. Generation of a squeezed state of an oscillator by stroboscopic back-action-evading measurement. *Nat. Phys.* **11**, 389–392 (2015).
28. Guerrero, A. M. et al. Quantum noise correlations of an optical parametric oscillator based on a nondegenerate four wave mixing process in hot alkali atoms. *Phys. Rev. Lett.* **125**, 083601 (2020).
29. Wu, H., Gea-Banacloche, J. & Xiao, M. Observation of intracavity electromagnetically induced transparency and polariton resonances in a Doppler-broadened medium. *Phys. Rev. Lett.* **100**, 173602 (2008).
30. Cimmarusti, A. D. et al. Environment-assisted speed-up of the field evolution in cavity quantum electrodynamics. *Phys. Rev. Lett.* **114**, 233602 (2015).
31. Yang, S., Wang, X., Bao, X. & Pan, J. An efficient quantum light-matter interface with sub-second lifetime. *Nat. Photon.* **10**, 381–384 (2016).
32. Bimbar, E. et al. Homodyne tomography of a single photon retrieved on demand from a cavity-enhanced cold atom memory. *Phys. Rev. Lett.* **112**, 033601 (2014).
33. Tanji, H., Ghosh, S., Simon, J., Bloom, B. & Vuletić, V. Heralded single-magnon quantum memory for photon polarization states. *Phys. Rev. Lett.* **103**, 043601 (2009).
34. Heller, L., Farrera, P., Heinze, G. & de Riedmatten, H. Cold-atom temporally multiplexed quantum memory with cavity-enhanced noise suppression. *Phys. Rev. Lett.* **124**, 210504 (2020).
35. Bruss, D., Ekert, A. & Macchiavello, C. Optimal universal quantum cloning and state estimation. *Phys. Rev. Lett.* **81**, 2598 (1998).
36. Hammerer, K., Wolf, M. M., Polzik, E. S. & Cirac, J. I. Quantum benchmark for storage and transmission of coherent states. *Phys. Rev. Lett.* **94**, 150503 (2005).
37. Bachor, H. A. & Ralph, T. C. A *Guide to Experiments in Quantum Optics* (Wiley-VCH, Weinheim, Berlin, 2004).
38. Ou, Z. Efficient conversion between photons and between photon and atom by stimulated emission. *Phys. Rev. A* **78**, 023819 (2008).
39. He, Q., Reid, M. D., Giacobino, E., Cviklinski, J. & Drummond, P. D. Dynamical oscillator-cavity model for quantum memories. *Phys. Rev. A* **79**, 022310 (2009).
40. Yan, Z., Liu, Y., Yan, J. & Jia, X. Deterministically entangling multiple remote quantum memories inside an optical cavity. *Phys. Rev. A* **97**, 013856 (2018).
41. Dur, W. & Cirac, J. I. Multiparty teleportation. *J. Mod. Opt.* **47**, 267 (2000).
42. Julsgaard, B., Sherson, J., Cirac, J. I., Fiurasek, J. & Polzik, E. S. Experimental demonstration of quantum memory for light. *Nature* **432**, 482–486 (2004).
43. Phillips, D. F., Fleischhauer, A., Mair, A., Walsworth, R. L. & Lukin, M. D. Storage of light in atomic vapor. *Phys. Rev. Lett.* **86**, 783 (2001).
44. Jensen, K. et al. Quantum memory for entangled continuous-variable states. *Nat. Phys.* **7**, 13–16 (2011).
45. Langer, C. et al. Long-lived qubit memory using atomic ions. *Phys. Rev. Lett.* **95**, 060502 (2005).
46. Casabone, B. et al. Enhanced quantum interface with collective ion-cavity coupling. *Phys. Rev. Lett.* **114**, 023602 (2015).
47. Hucul, D. et al. Modular entanglement of atomic qubits using photons and phonons. *Nat. Phys.* **11**, 37–42 (2014).
48. Wang, Y. et al. Single-qubit quantum memory exceeding ten-minute coherence time. *Nat. Photon.* **11**, 646–650 (2017).
49. Flurin, E., Roch, N., Pillet, J. D., Mallet, F. & Huard, B. Superconducting quantum node for entanglement and storage of microwave radiation. *Phys. Rev. Lett.* **114**, 090503 (2015).
50. Sillanpaa, M. A. et al. Autler-Townes effect in a superconducting three-level system. *Phys. Rev. Lett.* **103**, 193601 (2009).
51. Abdumalikov, A. A. et al. Electromagnetically induced transparency on a single artificial atom. *Phys. Rev. Lett.* **104**, 193601 (2010).
52. Clausen, C., Bussièrès, F., Afzelius, M. & Gisin, N. Quantum storage of heralded polarization qubits in birefringent and anisotropically absorbing materials. *Phys. Rev. Lett.* **108**, 190503 (2012).
53. Gündoğan, M., Ledingham, P. M., Almasi, A., Cristiani, M. & de Riedmatten, H. Quantum storage of a photonic polarization qubit in a solid. *Phys. Rev. Lett.* **108**, 190504 (2012).
54. Ma, Y., Ma, Y., Zhou, Z., Li, C. & Guo, G. One-hour coherent optical storage in an atomic frequency comb memory. *Nat. Commun.* **12**, 2381 (2021).
55. Zhong, M. et al. Optically addressable nuclear spins in a solid with a six-hour coherence time. *Nature* **517**, 177–180 (2015).
56. Fiore, V. et al. Storing optical information as a mechanical excitation in a silica optomechanical resonator. *Phys. Rev. Lett.* **107**, 133601 (2011).
57. Lee, H. et al. Spiral resonators for on-chip laser frequency stabilization. *Nat. Commun.* **4**, 2468 (2013).
58. Riedinger, R. et al. Non-classical correlations between single photons and phonons from a mechanical oscillator. *Nature* **530**, 313–316 (2016).
59. Kiesewetter, S., Teh, R. Y., Drummond, P. D. & Reid, M. D. Pulsed entanglement of two optomechanical oscillators and Furry’s hypothesis. *Phys. Rev. Lett.* **119**, 023601 (2017).
60. Safavi-Naeini, A. H. et al. Electromagnetically induced transparency and slow light with optomechanics. *Nature* **472**, 69–73 (2011).
61. Huo, M. et al. Deterministic quantum teleportation through fiber channels. *Sci. Adv.* **4**, eaas9401 (2018).
62. Jing, J. et al. Experimental demonstration of tripartite entanglement and controlled dense coding for continuous variables. *Phys. Rev. Lett.* **90**, 167903 (2003).
63. Steinlechner, S. et al. Quantum-dense metrology. *Nat. Photon.* **7**, 626–630 (2013).
64. Xu, Z. et al. Long lifetime and high-fidelity quantum memory of photonic polarization qubit by lifting Zeeman degeneracy. *Phys. Rev. Lett.* **111**, 240503 (2013).
65. Hedges, M. P., Longdell, J. J., Li, Y. & Sellars, M. J. Efficient quantum memory for light. *Nature* **465**, 1052–1056 (2010).
66. Zuo, X. et al. Quantum interferometer combining squeezing and parametric amplification. *Phys. Rev. Lett.* **124**, 173602 (2020).
67. Zhou, Y. et al. Quantum secret sharing among four players using multipartite bound entanglement of an optical field. *Phys. Rev. Lett.* **121**, 150502 (2018).
68. Guo, J. et al. High-performance Raman quantum memory with optimal control in room temperature atoms. *Nat. Commun.* **10**, 148 (2019).
69. Finkelstein, R. et al. Continuous protection of a collective state from inhomogeneous dephasing. *Phys. Rev. X* **11**, 011008 (2021).

## Acknowledgements

We thank Luis A. Orozco for the helpful discussion. The work was supported by the National Natural Science Foundation of China (Grants No. 62122044 (Z.Y.), No. 61925503 (X.J.), No. 11904218 (X.J.), No. 12147215 (X.J.), No. 61775127 (Z.Y.) and No. 11834010 (Z.Y.)), the Key Project of the National Key R&D program of China (Grant No. 2016YFA0301402 (X.J., Z.Y., C.X., K.P.)), the Program for the Innovative Talents of Higher Education Institutions of Shanxi (X.J.), the Program for the Outstanding Innovative Teams of Higher Learning Institutions of Shanxi (Z.Y.) and the fund for Shanxi “1331 Project” Key Subjects Construction (X.J., Z.Y., C.X., K.P.).

## Author contributions

Z.Y., X.J. and C.X. conceived the original idea. L.M., X.L., Z.Y., X.J. and K.P. designed the experiment. L.M., X.L., J.Y., R.L. and T.C. constructed and performed the experiment.

L.M., X.L., Z.Y. and X.J. accomplished theoretical calculation and the data analysis. Z.Y., X.J., C.X. and K.P. wrote the paper. All the authors reviewed the manuscript.

### Competing interests

The authors declare no competing interests.

### Additional information

**Supplementary information** The online version contains supplementary material available at <https://doi.org/10.1038/s41467-022-30077-1>.

**Correspondence** and requests for materials should be addressed to Zhihui Yan or Xiaojun Jia.

**Peer review information** *Nature Communications* thanks XYZ and the other, anonymous, reviewer(s) for their contribution to the peer review of this work.

**Reprints and permission information** is available at <http://www.nature.com/reprints>

**Publisher's note** Springer Nature remains neutral with regard to jurisdictional claims in published maps and institutional affiliations.



**Open Access** This article is licensed under a Creative Commons Attribution 4.0 International License, which permits use, sharing, adaptation, distribution and reproduction in any medium or format, as long as you give appropriate credit to the original author(s) and the source, provide a link to the Creative Commons license, and indicate if changes were made. The images or other third party material in this article are included in the article's Creative Commons license, unless indicated otherwise in a credit line to the material. If material is not included in the article's Creative Commons license and your intended use is not permitted by statutory regulation or exceeds the permitted use, you will need to obtain permission directly from the copyright holder. To view a copy of this license, visit <http://creativecommons.org/licenses/by/4.0/>.

© The Author(s) 2022